

Plaquette-centered rotation symmetry and octet-nodal superconductivity in KFe_2As_2

Guo-Yi Zhu¹ and Guang-Ming Zhang^{1,2}

¹*State Key Laboratory of Low-Dimensional Quantum Physics and*

Department of Physics, Tsinghua University, Beijing 100084, China.

²*Collaborative Innovation Center of Quantum Matter, Beijing 100084, China.*

(Dated: December 14, 2024)

In this paper, we first identify the plaquette-centered rotation symmetry C_4^p , which is found to stabilize the Fermi-surface structure of Fe-based superconductors. Together with the S_4 symmetry previously found by Hu and Hao (Phys. Rev. X **2**, 021009 (2012)), we are able to solve the puzzle of pairing symmetry of superconductivity in KFe_2As_2 in a simple but comprehensive way. By modeling the material with a strong coupling $t - J_1 - J_2$ model, we find phase transitions of pairing symmetry driven by the competition between the local spin antiferromagnetic couplings from nodal $d \times s$ -wave to nodeless s_{\pm} -wave through a narrow intermediate $s_{\pm} + id \times s$ mixed pairing phase, in consistent with the pressure experiment conducted by Taillefer's group (Nature Physics **9**, 349 (2013)). While the hole Fermi pockets around the Brillouin zone center usually give rise to nodeless s -wave Cooper pairing, the emergent d -wave form factor arises from the projection of inter-orbital Cooper pairing onto the Fermi surface determined by the C_4^p symmetry. Moreover, the S_4 symmetry dictates 2 copies of d -wave pairing condensates, counting 8 nodes in total. We further show that weakly breaking C_4^p naturally leads to the octet nodal gap as precisely observed in laser angle resolved photoemission spectroscopy. Neither accidental nor due to high angular momentum of Cooper pairs, the octet nodes can be attributed to a symbolic equation " $8 = 4 + 4$ ", which reflects the interplay between the C_4^p and S_4 symmetries and sheds new light on the enigma of the pairing symmetry in KFe_2As_2 . Therefore, our theory highlights the multi-orbital characters of Fe-based superconductors, and the perfect agreement with experiments demonstrates the significant roles played by both C_4^p and S_4 symmetries in organizing the tangling Fe orbitals in the manner of simplicity and universality.

I. INTRODUCTION

As the first family of high temperature superconductivity (SC), the cuprates have been under elaborate studies for nearly thirty years[1–4], and a consensus has been reached by the majority of condensed matter physicists that the intriguing superconducting phase of cuprates are rooted in the electronic strong antiferromagnetic (AF) correlation. The SC in optimally doped compounds is confirmed by a vast majority of theories and experiments to be d -wave pairing symmetry[5–7]. For the theorists, the complex reality arising from both the $3d$ orbital on Cu ions and $2p$ orbital on O ions are compromised by the Zhang-Rice singlets, which result in a rather successful description of a single-band model for the cuprates - the celebrated t-J model[3, 4, 8–10].

Distinct from the cuprates, the family of Fe-based superconductors has a seemingly less unified picture as to their Fermi surface (FS) structure, pairing symmetries and pairing glues[11]. From the perspective of band structure, they owe their complexity to the multi-orbital character. Some Fermi pockets could vanish under doping or pressure and are less robust than the others[12, 13]. Regarding the pairing symmetry, the s_{\pm} -wave pairing symmetry has been established for many iron-pnictides from different approaches[14–16], but it fails to account for all the materials observed experimentally. When it comes to the interactions responsible for pairing, there are weak coupling theories that count on the antiferromagnetic spin fluctuation[14] or orbital fluctuation to

work as the pairing glue, but they are less satisfying when FS nesting is absent, or when there exists strong correlation between local magnetic moments[11]. For all these considerations, we are still in need of a strong coupling theory to accommodate the antiferromagnetic spin fluctuation.

The representative of heavily hole doped $\text{Ba}_{1-x}\text{K}_x\text{Fe}_2\text{As}_2$ family - KFe_2As_2 is a particular intriguing case among the Fe-based superconductors, regarding its pairing symmetry and interaction. Angle resolved photoemission spectroscopy (ARPES) experiments[12, 13] report the absence of electron pockets and leave only three hole Fermi pockets around the Brillouin zone (BZ) center (Γ point). Usually this suggests nodeless s -wave pairing symmetry. But it turns out that nodal gap structure was indicated by thermal conductivity measurement[17], penetration depth measurement[18], and NMR probe[19–21]. The d -wave pairing symmetry was then proposed after functional renormalization group calculation[22], which was supported by the measurement of heat conduction[23]. Later on Okazaki et. al. utilized the ultra-high energy resolution of laser ARPES to map the gap structure much more explicitly[24]. Quite dramatically, their report showed octet nodal gap on the middle hole pocket while nodeless gap on the inner hole pocket, in striking contrast to the theoretical expectation. Then there were attempts to resort to accidental nodes to account for the octet nodes. But as far as we are concerned, the nodes robustly observed in various experiments deserve

far more convincing explanation.

Meanwhile, we notice another experiment that is relevant to the pairing symmetry: Taillefer's group reported their study on KFe_2As_2 under tuning pressure[25], in which they witnessed a non-monotonic V-shaped tendency of the critical temperature with increasing pressure. Their results indicated a phase transition near the point of the sudden change of T_c . The possibility of FS transition was ruled out by their Hall coefficient measurement, pointing towards a phase transition of pairing symmetry. Since the main ingredients determining the pairing symmetry are the FS structure and the electronic interactions responsible for pairing, it can be concluded that the phase transitions are essentially driven by the competition between the local spin AF exchanges, because the FS remains almost the same. And we also notice that the KFe_2As_2 is regarded as a strongly correlated system evidenced by the remarkable mass enhancement[12, 26] and highly incoherent spectral weight[27]. Therefore a strong AF coupling model with tunable interactions is in need.

To model the Fe-based SCs, we have to understand the electronic structure firstly. There have been many theoretical treatments by taking all five or even ten $3d$ -orbitals of Fe into consideration, but the necessity for such a huge parameter space is hardly conceivable, because the pairing symmetries are so robust[28]. From this point of view, we especially appreciate the S_4 symmetry found by Hu and Hao[29], which provides a rational way to sort out the tangling multi-orbitals of Fe-based SCs. In the presence of S_4 , the band structure of multi-orbitals is then reduced to a minimal two-band model. Despite owning a few parameters, the model based on S_4 symmetry is capable of accommodating most FS structures of both iron-pnictides and iron-chalcogenides[29], potentially hopeful to unify the electronic structure of Fe-based SCs. However, they only focused on the symmetric nearest neighbor hopping in their model, leaving behind the heavily hole doped limit of iron-pnictides KFe_2As_2 , where only hole pockets are present.

In this paper we first identify the plaquette-centered rotation symmetry C_4^p , which is complementary to the S_4 symmetry in providing a simple and potentially universal organizing principle for the tangling orbitals of Fe-based superconductors. We show that, while S_4 plays the role of organizing two groups of orbitals, C_4^p is responsible for stabilizing the FS structure of iron-pnictides, including the heavily hole doped limit where the electron Fermi pockets at X are absent. A different representation of this plaquette-centered rotation symmetry \tilde{C}_4^p can stabilize the FS structure of iron-chalcogenides, including the monolayer FeSe on SrTiO_3 substrate where a tiny hole Fermi pocket around Γ vanishes[30, 31]. Therefore, both families of Fe-based superconductors share the plaquette-centered rotation symmetry, at least approximately. Returning to the case of KFe_2As_2 , the joint cooperation of

the S_4 and C_4^p symmetries manifest its power particularly in settling the controversy of pairing symmetry and nodeness in this material.

To study the pairing symmetry of SC in KFe_2As_2 , we take the strong coupling approach as the starting point by modeling this material with the $t - J_1 - J_2$ model subjected to the particle occupancy constraint, in contrast to the models with the on-site Coulomb repulsion and Hund's coupling. Within the slave-boson mean-field approximation, we find that, by decreasing the ratio of J_1/J_2 , the KFe_2As_2 samples could experience phase transitions of pairing symmetry from the $d \times s$ -wave SC to s_{\pm} -wave SC through a narrow intermediate $s_{\pm} + id \times s$ mixed pairing phase, consistent with pressure experiment[25]. The d -wave form factor emerges from the renormalization effect of the orbital hybridization in the representation of C_4^p and becomes the characteristic nature of a multi-orbital superconductors. The renormalization effect is similar to the mechanism of inducing effective intraband p -wave pairing upon helical electrons by imposing s -wave singlet pairing[32]. Moreover, together with the S_4 symmetry, we are in fact bestowed with 2 copies of d -wave gap structure, counting 8 nodes in total. By weakly breaking C_4^p we are naturally led to the so-called "octet-noded monster" observed by laser ARPES. We thus propose a symbolic equation " $8 = 4 + 4$ " that captures the essential physics ruled by S_4 and C_4^p symmetries, exhibiting the origin of nodes in a rather simple and comprehensive way.

II. C_4^p SYMMETRY AND BAND TOPOLOGY

Due to the weak out-of-plane tunneling (along c -axis), the electronic properties of Fe-based SCs are mainly contained in the FeAs plane, where the Fe atoms form a square lattice and the As atoms alternate above or below the Fe plaquette center (Fig.1a). Because of the checkerboard pattern of As lattice, the FeAs plane does not respect the site-centered C_4^s symmetry, but is invariant under the site-centered C_4^s rotation followed by a mirror reflection with respect to the plane[29]: $S_4 \equiv C_4^s \times R_z$. But we further notice that the plaquette-centered rotation symmetry C_4^p is preserved by the lattice. Among the five d -orbitals, the low-energy physics near the FS is mainly contributed by the d_{xz}, d_{yz}, d_{xy} orbitals. Instead of a direct tunneling via the wave function overlap, the hopping between d_{xz} - and d_{yz} -orbitals is primarily contributed by their hybridization with the p -orbitals on the As atoms, whereas the d_{xy} orbitals do not have this privilege and are not included in our minimal model. The As atoms on plaquette centers polarize the d_{xz} - and d_{yz} -orbitals into $d_{x'z}$ - and $d_{y'z}$ -orbitals to maximize energy gain from hopping (Fig.1a and Fig.1b). Therefore the square lattice with $d_{x'z}$ and $d_{y'z}$ orbitals on each site is effectively factorized into the top and bottom layers

where each site has one orbital but the unit cell has to be doubled.

As shown in Fig.1b, the top layer has $d_{x'z}$ living on the odd lattice sites (denoted as A) and $d_{y'z}$ on the even lattice sites (denoted as B). Likewise, the bottom layer has $d_{y'z}$ living on the odd lattice sites (denoted as C) and $d_{x'z}$ on the even lattice sites (denoted as D). For convenience we will denote the top layer as "AB layer" while the bottom layer as "CD layer". Albeit weakly coupled by inter-layer tunneling, the two layers are related by the S_4 symmetry, while the sublattice degrees of freedom inside each layer are rotated by C_4^p . To demonstrate the symmetries, we introduce the notion $\tau_{\mu\nu} \equiv I_\mu \otimes I_\nu$, $\mu, \nu = 0, 1, 2, 3$, where the first Pauli matrix I_μ acts on the S_4 spinor space spanned by those states living on either layer, and the latter Pauli matrix I_ν acts on the C_4^p spinor space composed of states living on each sublattice. By choosing the simple gauge as shown in Fig.1b, the representation of S_4 and C_4^p symmetries can be explicitly expressed as

$$S_4 : \begin{pmatrix} A_{\mathbf{k},\sigma} \\ B_{\mathbf{k},\sigma} \\ C_{\mathbf{k},\sigma} \\ D_{\mathbf{k},\sigma} \end{pmatrix} \rightarrow \begin{pmatrix} C_{\mathbf{k}',\sigma} \\ -D_{\mathbf{k}',\sigma} \\ -A_{\mathbf{k}',\sigma} \\ B_{\mathbf{k}',\sigma} \end{pmatrix} = i\tau_{23} \begin{pmatrix} A_{\mathbf{k}',\sigma} \\ B_{\mathbf{k}',\sigma} \\ C_{\mathbf{k}',\sigma} \\ D_{\mathbf{k}',\sigma} \end{pmatrix},$$

$$C_4^p : \begin{pmatrix} A_{\mathbf{k},\sigma} \\ B_{\mathbf{k},\sigma} \\ C_{\mathbf{k},\sigma} \\ D_{\mathbf{k},\sigma} \end{pmatrix} \rightarrow \begin{pmatrix} B_{\mathbf{k}',\sigma} \\ -A_{\mathbf{k}',\sigma} \\ -D_{\mathbf{k}',\sigma} \\ C_{\mathbf{k}',\sigma} \end{pmatrix} = i\tau_{32} \begin{pmatrix} A_{\mathbf{k}',\sigma} \\ B_{\mathbf{k}',\sigma} \\ C_{\mathbf{k}',\sigma} \\ D_{\mathbf{k}',\sigma} \end{pmatrix},$$

where $\mathbf{k}' = C_4\mathbf{k}$. Since the spin-orbit coupling is not concerned so that spin degeneracy is always present, the rotation factor contributed by the spin rotation $(1 + i\sigma_z)/\sqrt{2}$ does not affect the physics and can be absorbed by a basis transformation. Moreover, we would like to point out that these two symmetries commute with each other.

Formally, the C_4^p symmetry operation is indeed diagonal in the S_4 spinor space and mainly rotates the intra-layer sublattices, while the S_4 operation is diagonal in each sublattice but primarily rotates the layers. It is worth noticing that the S_4 spinor and C_4^p spinor look like dual to each other. But the inter-sublattice hopping is much stronger than the inter-layer tunneling, which makes the S_4 doublet weakly coupled but C_4^p doublet strongly hybridized. The power of the S_4 symmetry lies in that, once the dynamics of one layer is obtained, it is straightforward to derive the other. Therefore, in the presence of S_4 , we are bestowed with a minimal C_4^p spinor model living on either layer. In the following we focus on the properties of the top layer before paying a revisit to the complete S_4 spinor.

As shown in Fig.1b, the kinetic part of the model Hamiltonian mainly involves anisotropic nearest neighbor (NN) hopping t_1 and the next nearest neighbor (NNN) hopping t_2 or t'_2 , which can be recombined and decomposed into s -wave and d -wave representation: $t_{1s} =$

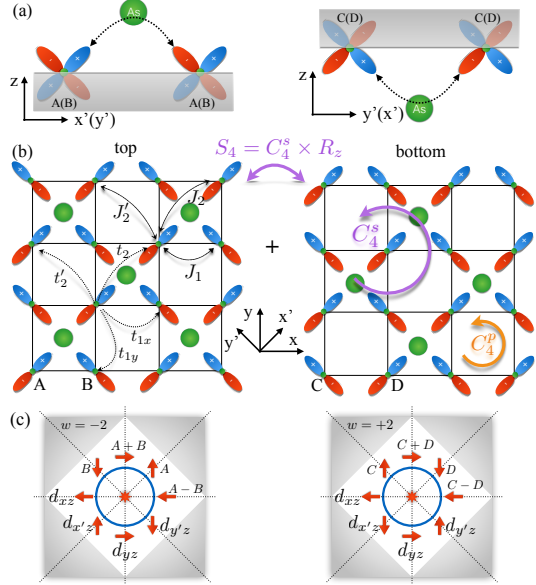


FIG. 1: Lattice configuration of the iron-pnictides. (a) The transverse view of the Fe-As plane shows the hopping of $3d_{x'(y')z}$ orbital via hybridization with $p_{x'(y')}$ orbital on arsenic atoms, either above or below the Fe square lattice plane. (b) The $3d_{x'(y')z}$ orbitals on the Fe lattice can be approximately decoupled into two groups which hop around via the arsenic atom on top or bottom of the plane respectively. Thus the lattice can be viewed as "factorized" into the top and bottom layers, which are related by S_4 symmetry. (c) For d -wave representation of plaquette-centered rotation symmetry C_4^p , the Γ point is the source of Berry flux carrying topological winding number $w = \mp 2$ for AB (CD) layer. The red arrow denotes the polarization of C_4^p spinor on the Fermi pocket, where spin up represents A(C) orbitals and spin down represents B(D) orbitals.

$(t_{1x} + t_{1y})/2$, $t_{1d} = (t_{1x} - t_{1y})/2$, $t_{2s} = (t_2 + t'_2)/2$, and $t_{2d} = (t_2 - t'_2)/2$. In terms of the C_4^p spinor $\Psi_{\mathbf{k},\sigma} \equiv (A_{\mathbf{k},\sigma}, B_{\mathbf{k},\sigma})^T$, it is then expressed as

$$H_t^{\text{AB}} = \frac{1}{2} \sum_{\mathbf{k},\sigma} \Psi_{\mathbf{k},\sigma}^\dagger [\epsilon_0(\mathbf{k}) + \epsilon_x(\mathbf{k})I_1 + \epsilon_z(\mathbf{k})I_3] \Psi_{\mathbf{k},\sigma}, \quad (1)$$

where \mathbf{k} ranges in the unfolded BZ and

$$\begin{aligned} \epsilon_0(\mathbf{k}) &= 4t_{2s} \cos k_x \cos k_y - \mu, \\ \epsilon_z(\mathbf{k}) &= -4t_{2d} \sin k_x \sin k_y, \\ \epsilon_x(\mathbf{k}) &= 2t_{1d} (\cos k_x - \cos k_y) + 2t_{1s} (\cos k_x + \cos k_y) \\ &\equiv \epsilon_{xd}(\mathbf{k}) + \epsilon_{xs}(\mathbf{k}). \end{aligned} \quad (2)$$

Note that $\epsilon_z(\mathbf{k})$ denotes the sublattice energy difference and $\epsilon_x(\mathbf{k})$ is the energy gain from the NN hopping process. A vector can be defined by $\mathbf{h}(\mathbf{k}) \equiv (\epsilon_x, 0, \epsilon_z)$, which acts as a "magnetic field" living in the momentum space and pinning the C_4^p spinor (Fig.1c). It should be noted that in AB layer the sublattice degree of freedom is locked with the atomic internal angular momentum i.e. odd site

carrying $d_{x'z}$ while even site carrying $d_{y'z}$, so that the C_4^p spinor is actually a composite of the sublattice degree of freedom and the internal atomic angular momentum. For instance, when $t_{1s} = 0$, $t_{1d} < 0$, $t_{2s} > 0$, $t_{2d} > 0$, the spinor along k_x with the lowest energy is composed of the equal superposition of $d_{x'z}$ -orbitals on odd sites and $d_{y'z}$ -orbitals on even sites (Fig.1c), which is equivalent to d_{xz} -orbitals. And along the BZ diagonal, the spinor with the lowest energy consists of the $d_{x'z}$ -orbitals on odd sites or $d_{y'z}$ -orbitals on even sites.

Before diagonalization, there are several remarks about the symmetries in this kinetic part. The d -wave and s -wave NN hopping correspond to two distinctive symmetry representations of the plaquette-centered rotation symmetry. Without loss of generality, we assume that both t_{1s} and t_{1d} have finite values. Based on the sketch of a snapshot of the wave function distribution in Fig.1b, we naturally expect $|t_{1d}| \gg |t_{1s}| \approx 0$. Indeed, adding a nonzero t_{1s} would break the symmetry C_4^p :

$$C_4^{p\dagger} [\epsilon_{xd}(\mathbf{k}) + \epsilon_{xs}(\mathbf{k})] I_1 C_4^p = [\epsilon_{xd}(\mathbf{k}) - \epsilon_{hs}(\mathbf{k})] I_1. \quad (3)$$

So the ideal case of $t_{1s} = 0$ and $t_{1d} \neq 0$ respects the symmetry C_4^p , which can faithfully characterize the FS structure of iron-pnictides. Nevertheless, the other limit of $t_{1d} = 0$ and $t_{1s} \neq 0$ restores the plaquette-centered rotation symmetry with a distinct representation $\tilde{C}_4^p \equiv \tau_{31}$, capturing the FS structure of iron-chalcogenides.

In the helicity basis, H_t^{AB} can be directly diagonalized

$$H_t^{\text{AB}} = \frac{1}{2} \sum_{\mathbf{k},\sigma} \left[\xi_e(\mathbf{k}) \alpha_{\mathbf{k},\sigma}^\dagger \alpha_{\mathbf{k},\sigma} + \xi_h(\mathbf{k}) \beta_{\mathbf{k},\sigma}^\dagger \beta_{\mathbf{k},\sigma} \right], \quad (4)$$

where $\xi_{e(h)}(\mathbf{k}) = \epsilon_0 \pm \sqrt{\epsilon_x^2 + \epsilon_z^2}$ represents the electron (hole) band with \pm helicity, respectively:

$$\begin{aligned} \alpha_{\mathbf{k},\sigma}^\dagger &= \left(\cos \frac{\theta_{\mathbf{k}}}{2} \right) A_{\mathbf{k},\sigma}^\dagger + \text{sgn}(\epsilon_x) \left(\sin \frac{\theta_{\mathbf{k}}}{2} \right) B_{\mathbf{k},\sigma}^\dagger, \\ \beta_{\mathbf{k},\sigma}^\dagger &= \left(\cos \frac{\theta_{\mathbf{k}}}{2} \right) B_{\mathbf{k},\sigma}^\dagger - \text{sgn}(\epsilon_x) \left(\sin \frac{\theta_{\mathbf{k}}}{2} \right) A_{\mathbf{k},\sigma}^\dagger, \end{aligned} \quad (5)$$

and the hybridization angle is given by $\theta_{\mathbf{k}} = \tan^{-1} \frac{|\epsilon_x|}{\epsilon_z} \in [0, \pi]$. The band dispersion and the corresponding FS structures can be easily obtained. Fig.2a exhibits the coexistence of a hole pocket around Γ and an electron pocket around X point in the absence of the s -wave NN hopping, a characteristic FS structure of most iron-pnictides. As the d -wave NN hopping is growing, the electron band is gradually pushed upwards, shrinking the electron pocket. It finally leads to the FS structure of KFe_2As_2 (Fig.2b), where the electron pocket completely vanishes. This evolution can be related to the doping process of $\text{Ba}_{1-x}\text{K}_x\text{Fe}_2\text{As}_2$ iron-pnictides[33].

Note that the shape of the hole pocket is C_4 symmetric thanks to the symmetry C_4^p , and the two bands touch each other quadratically at zone center Γ point, which is

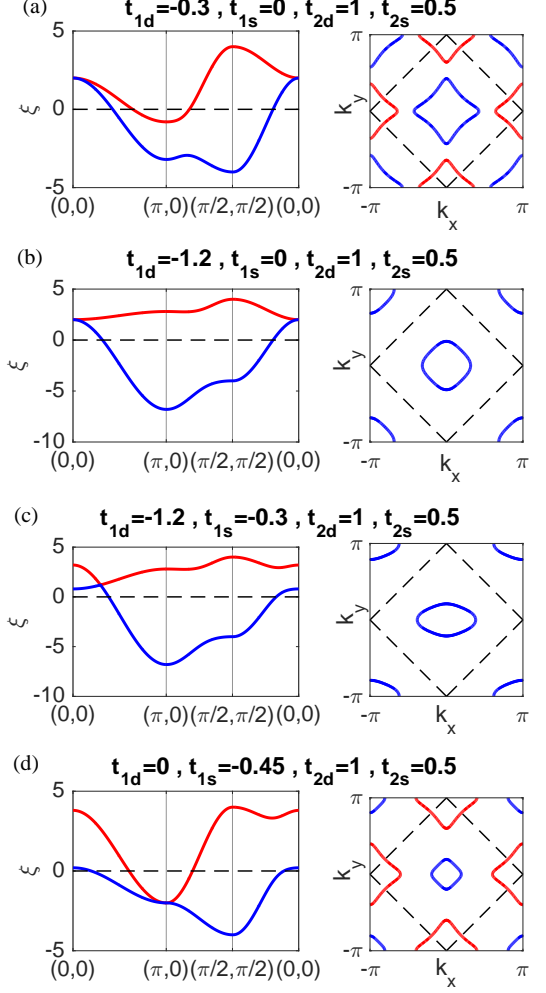


FIG. 2: Band structures and Fermi surfaces of the minimal model without considering any electron interactions for various systems of Fe-based superconductors. Left panel shows the band structure for varying parameters while right panel shows the corresponding FS in the unfolded BZ. (a) Hole pocket is located around Γ and electron pocket around X , describing the FS structure for iron-pnictides. The Γ point is a double Dirac point with quadratic band touching dispersion. (b) Electron pocket vanishes, while the hole pocket around Γ is robust, standing for the heavily hole doped iron-pnictides. (c) Mixing d -wave NN hopping with s -wave component can split the double Dirac point into two Dirac points while elongating the hole pocket. Hole pocket could be further torn apart. (d) Replacing pure d -wave NN hopping with s -wave one is equivalent to a gauge transform combined with a particle-hole transform, as a result the double Dirac point is shifted to the folded BZ corner X , stabilizing an electron pocket instead and vanishing the hole pocket.

not accidental but rather due to the topological nature related with C_4^p symmetry. Namely the helical spinor is pinned by $\mathbf{h}(\mathbf{k})$ to wind around the Γ point twice, yielding a topological number $w = 2\text{sgn}(t_{1d}t_{2d})$ (Ref.[34]). It is this topological number that forces the electron and hole bands to touch quadratically at the vortex core of $\mathbf{h}(\mathbf{k})$,

i.e. the Γ point, which becomes the source of the Berry flux experienced by the helical spinor (see Fig.1c). Consequently, the hole pocket surrounding the vortex core is protected by topology, whereas the electron pocket is less robust. As long as the time reversal (TR) symmetry is present, the occurrence of I_2 is forbidden and this vortex core is robust. However, the TR symmetry cannot prevent the double Dirac point at Γ from splitting apart into two Dirac nodes, which could be driven by a C_4^p -breaking term. This is indeed the case when the s -wave hoping comes in mixing the d -wave NN hopping (Fig.2c), where the hole pocket experiences a "nematic force" and is simultaneously elongated. When the C_4^p symmetry breaking term is large enough, the hole pocket around Γ is going to be torn apart, resulting in two pockets surrounding the Dirac nodes, which is irrelevant to the real materials. So the iron-pnictides with hole pockets around Γ robustly observed in experiments must preserve the C_4^p symmetry, at least approximately. In other words, the FS structure of iron-pnictides is stabilized by the C_4^p symmetry which helps the TR symmetry protect and confine the double Dirac point to the hole pocket center. In this sense, the C_4^p symmetry is one of the key relevant features of iron-pnictides, which can tolerate only tiny amount of s -wave hoping that weakly breaks C_4^p symmetry.

In Fig.2d, we also show that, when the d -wave NN hopping is completely replaced by the s -wave hoping, the model gives rise to the FS with a robust electron pocket around X point but without hole pocket around Γ , which is characteristic of iron-chalcogenides[35]. Such a choice of parameters corresponds to a rather different gauge choice (see Appendix A), and the representation of the plaquette-centered rotation symmetry is correspondingly modified by $\tilde{C}_4^p \equiv \tau_{31}$. In this case, the electron pocket and its central double Dirac point are protected by the TR symmetry together with the symmetry \tilde{C}_4^p instead. It is worth noticing that the band structure of iron-chalcogenides is related to that of iron-pnictides by a gauge transform combined with a particle-hole transform.

Therefore, the FS structures of iron-pnictides and iron-chalcogenides are both topologically protected by the plaquette-centered rotation symmetry, though they differ by the specific representation either C_4^p or \tilde{C}_4^p . And the protecting mechanism tolerates a weak symmetry breaking term. In the next section, we will focus on the d -wave NN hopping limit by sending $t_{1s} \rightarrow 0$ for KFe_2As_2 . Specifically, we can choose the realistic hopping parameters as $t_{1d} = -1.2$, $t_2 = 1.5$, and $t'_2 = -0.5$, whose corresponding band structure is given by Fig.2b. When things are clear in the ideal case, we will reintroduce a weak s -wave NN hopping to model the more realistic material later on.

III. C_4^p -PROTECTED d -WAVE RENORMALIZED PAIRING SC

A. Strong coupling model and treatment

Provided the electronic structure, we need to include the electronic interactions. The strong correlation effect of KFe_2As_2 evidenced by experiments [12, 26, 27] asks for a strong coupling approach. Particularly, the optical measurement[27] had showed the incoherent spectral weight of KFe_2As_2 as high as 10% hole-doped $\text{La}_{2-x}\text{Sr}_x\text{CuO}_4$, revealing the strong antiferromagnetic correlation similar to the cuprates. Therefore, we would like to model this system with AF super-exchanges containing the NN and NNN interactions as shown in Fig.1b, similar to the effective description of cuprates. However, distinct from the $t - J_1 - J_2$ model in [15], our kinetic part of the model Hamiltonian is subjected to the projection that projects out double-occupancy. The projector is indispensable to capturing the strong AF correlation, reminding the electrons of their local nature rather than itinerant. Thus, we arrive at the model Hamiltonian for AB layer $H_J^{\text{AB}} = \mathcal{P}H_t^{\text{AB}}\mathcal{P} + H_J^{\text{AB}}$ with interaction terms:

$$H_J^{\text{AB}} = J_1 \sum_{\mathbf{r}, \delta} S_{\mathbf{r}}^A \cdot S_{\mathbf{r}+\delta}^B + J_2 \sum_{\mathbf{r}} (S_{\mathbf{r}}^A \cdot S_{\mathbf{r}+(\hat{x}+\hat{y})}^A + S_{\mathbf{r}}^B \cdot S_{\mathbf{r}+(\hat{x}+\hat{y})}^B) + J'_2 \sum_{\mathbf{r}} (S_{\mathbf{r}}^A \cdot S_{\mathbf{r}+(\hat{x}-\hat{y})}^A + S_{\mathbf{r}}^B \cdot S_{\mathbf{r}+(\hat{x}-\hat{y})}^B), \quad (6)$$

where $\delta = \pm\hat{x}, \hat{y}$ is the NN vector. Note H_J^{CD} is also related to H_J^{AB} by S_4 symmetry. As the low-energy descendant of the on-site Hubbard interaction, the AF super-exchange J-terms rely on the corresponding hopping integrals. Like the case in cuprates, the parameters can be chosen as $J_2 = 0.5$ and $J'_2 = 0.2$ as roughly one third of the corresponding hopping integrals and the dopant concentration is fixed at 0.05, because the doping does not make any qualitative changes. Note that although J'_2 differs from J_2 , but as will be shown later only the combination $J_{2s} \equiv \frac{2J_2J'_2}{J_2+J'_2}$ contributes to pairing, so that the physics is essentially captured by the competition between J_1 and J_{2s} . The parameter J_1 is chosen as the tuning parameter that mimics the inverse pressure when being compared with the experiment[25]. The projector \mathcal{P} declares the particle occupancy constraints: $\sum_{\sigma} A_{\mathbf{r}, \sigma}^{\dagger} A_{\mathbf{r}, \sigma} \leq 1$ and $\sum_{\sigma} B_{\mathbf{r}, \sigma}^{\dagger} B_{\mathbf{r}, \sigma} \leq 1$, which lead to emergent spin-charge separation physics. To tackle the constraint, we adopt the well-established slave-boson decomposition to factorize electron into fermionic spinon and bosonic holon:

$$A_{\mathbf{r}, \sigma} = h_{\mathbf{r}}^{\dagger} a_{\mathbf{r}, \sigma}, B_{\mathbf{r}, \sigma} = h_{\mathbf{r}}^{\dagger} b_{\mathbf{r}, \sigma}, \quad (7)$$

in which way the constraint becomes equalities: $\sum_{\sigma} a_{\mathbf{r}, \sigma}^{\dagger} a_{\mathbf{r}, \sigma} + h_{\mathbf{r}}^{\dagger} h_{\mathbf{r}} = 1$ and $\sum_{\sigma} b_{\mathbf{r}, \sigma}^{\dagger} b_{\mathbf{r}, \sigma} + h_{\mathbf{r}}^{\dagger} h_{\mathbf{r}} = 1$,

and can be enforced via a Lagrangian multiplier. Meanwhile, by treating the bosonic holon on the mean-field level $\langle h_r^\dagger \rangle = \langle h_r \rangle = \sqrt{x}$, and introducing the uniform valence bond and singlet pairing order parameters

$$\kappa_{ij} = -\frac{J}{4} \left\langle \sum_{\sigma} a_{i,\sigma}^\dagger a_{j,\sigma} \right\rangle, \Delta_{ij} = \frac{J}{4} \langle a_{i,\uparrow} a_{j,\downarrow} - a_{i,\downarrow} a_{j,\uparrow} \rangle,$$

the interactions on the sublattice A can be decoupled into the valence bond channel and singlet pairing channel. Likewise for the interactions on the sublattice B, and those interactions between the two sublattices A and B. Moreover, the NN and NNN valence bond and singlet pairing order parameters in real space can be rearranged into the *s*-wave and *d*-wave representations:

$$\begin{aligned} \kappa_{2s} &= (\kappa_2 + \kappa'_2)/2, \quad \kappa_{2d} = (\kappa_2 - \kappa'_2)/2, \\ \Delta_{1s} &= (\Delta_{1x} + \Delta_{1y})/2, \quad \Delta_{1d} = (\Delta_{1x} - \Delta_{1y})/2, \\ \Delta_{2s} &= (\Delta_2 + \Delta'_2)/2, \quad \Delta_{2d} = (\Delta_2 - \Delta'_2)/2. \end{aligned} \quad (8)$$

Note that we have assumed the valence bond order maintains the C_4^p symmetry, so that κ_1 is automatically of *d*-wave symmetry.

Finally, a mean-field Hamiltonian can be obtained

$$H_{\text{MF}}^{\text{ab}} = H_t^{\text{ab}} + H_{\Delta}^{\text{ab}}, \quad (9)$$

which describes the spinon dynamics on the AB layer. The kinetic part H_t^{ab} describes spinons with the same band structure as we discussed in the last section. $H_t^{\text{AB}} \rightarrow H_t^{\text{ab}}$ requires replacing the electronic fermions with the corresponding slave spinons $\Psi_{\mathbf{k},\sigma} = (A_{\mathbf{k},\sigma}, B_{\mathbf{k},\sigma})^T \rightarrow \psi_{\mathbf{k},\sigma} \equiv (a_{\mathbf{k},\sigma}, b_{\mathbf{k},\sigma})^T$, while renormalizing the hopping integrals and the chemical potential as

$$\begin{aligned} t_{1d} &\rightarrow \tilde{t}_{1d} = (t_{1dx} + \kappa_1), \quad t_{1s} \rightarrow \tilde{t}_{1s} = t_{1sx}, \\ t_{2s} &\rightarrow \tilde{t}_{2s} = (t_{2sx} + \kappa_{2s}), \\ t_{2d} &\rightarrow \tilde{t}_{2d} = (t_{2dx} + \kappa_{2d}), \\ \mu_0 &\rightarrow \mu = \mu_0 - \lambda - (J_2 + J_3)/4. \end{aligned} \quad (10)$$

The hybridization relation Eq. (5) also holds by replacing A(B) with a(b), and the mean-field pairing terms can be compactly expressed in terms of the C_4^p spinor:

$$H_{\Delta}^{\text{ab}} = \frac{1}{2} \sum_{\mathbf{k}} \psi_{\mathbf{k},\uparrow}^\dagger (\Delta_0 + i\Delta_x I_x + \Delta_z I_z) (\psi_{\mathbf{k},\downarrow}^\dagger)^T + h.c. \quad (11)$$

with

$$\begin{aligned} \Delta_0(\mathbf{k}) &= 2\Delta_{2s} \cos k_x \cos k_y, \\ \Delta_z(\mathbf{k}) &= 2\Delta_{2d} \sin k_x \sin k_y, \\ \Delta_x(\mathbf{k}) &= \Delta_{1s} (\cos k_x + \cos k_y) + i\Delta_{1d} (\cos k_x - \cos k_y). \end{aligned}$$

Provided with all the form factors available from the interactions, we can eliminate some of them which are apparently unfavorable energetically. In this minimal

model for KFe₂As₂, within the AB layer, there is only a small hole pocket around Γ point without apparent FS nesting. The Cooper pair formed on the FS is more likely to be scattered onto the same FS with small momentum transfer. And the pairing interactions $J_1(q) \propto -2J_1(\cos q_x + \cos q_y)$, $J_{2s}(q) \propto -4J_{2s} \cos q_x \cos q_y$ are attractive when $q \approx 0$, while $J_{2d}(q) \propto 4J_{2d} \sin q_x \sin q_y$ tends to vanish at small momentum. Therefore the pairing components $\Delta_{xd} = \Delta_{1d} (\cos k_x - \cos k_y)$ and $\Delta_z = 2\Delta_{2d} \sin k_x \sin k_y$, whose nodal lines brutally cross the hole pocket FS, are energetically unfavorable when compared to $\Delta_{xs} = \Delta_{1s} (\cos k_x + \cos k_y)$ and $\Delta_0 = 2\Delta_{2s} \cos k_x \cos k_y$, which endow the FS with largest possible energy gain. In fact, we did some self-consistent calculation numerically to verify that indeed $\Delta_{1d} = \Delta_{2d} = 0$. Thus we are left with two *s*-wave pairing components Δ_{1s} and Δ_{2s} to be determined by minimizing the ground state energy. We will show in the following that the two pairing components are competing driven by their respective interaction sources.

B. Hole band projection and phase transitions

As there is only single hole pocket FS in the low energy excitations, we can project the effective Hamiltonian onto the hole band and especially focus on the vicinity of FS. Turned to the helicity basis $\Gamma_{\mathbf{k},\sigma} \equiv (\alpha_{\mathbf{k},\sigma}, \beta_{\mathbf{k},\sigma})^T$, the mean-field Hamiltonian can be straight forwardly projected as

$$\begin{aligned} H_{\text{eff}}^{\text{ab}} &= \frac{1}{2} \sum_{\mathbf{k},\sigma} \xi_h(\mathbf{k}) \beta_{\mathbf{k},\sigma}^\dagger \beta_{\mathbf{k},\sigma} \\ &+ \frac{1}{2} \sum_{\mathbf{k}} \left(\Delta_0(\mathbf{k}) - \frac{\epsilon_x(\mathbf{k})}{\sqrt{\epsilon_x^2 + \epsilon_z^2}} i\Delta_x(\mathbf{k}) \right) \beta_{\mathbf{k},\uparrow}^\dagger \beta_{-\mathbf{k},\downarrow}^\dagger + h.c. \end{aligned} \quad (12)$$

Here we can see that the *s*-wave pairing component Δ_x arising from the NN spin exchange interaction is renormalized by a *d*-wave form factor $\epsilon_x \propto (\cos k_x - \cos k_y)$, which is inherited from the NN hopping integral in the C_4^p symmetry representation. Actually it should be no surprise, since we can physically understand this renormalization factor in such a way: the NN pairing interaction glues the inter-sublattice particles, which coexist in the hole band with probability proportional to the hybridization energy gain, as a result the effective intra-hole-band pairing condensate is supposed to be renormalized by ϵ_x . To be more specific, as shown in Fig.1c, along the zero lines of hybridization energy ϵ_x there's no coexistence of the sublattice degrees of freedom, so that there are no inter-orbital Cooper pairs, regardless of their internal pairing symmetry. Actually such a mechanism is parallel to inducing effective intra-band *p*-wave pairing upon the helical electrons when *s*-wave singlet Cooper pair is formed[32].

Then the Bogoliubov quasi-particle spectrum is straight forward for this effective single band BdG Hamiltonian:

$$E(\mathbf{k}) = \pm \sqrt{\xi_h^2 + \Delta_0^2 + \frac{\epsilon_x^2}{\epsilon_x^2 + \epsilon_z^2} \Delta_x^2}, \quad (13)$$

which exhibits the nodal excitations when $\Delta_0 = 0$. Note that the inter-band pairing between hole band and high energy electron band contributes second order perturbation corrections to the gap structure, but is unable to alter its symmetry. The d -wave gap nodes carrying one unit of vorticity in the Nambu space are topologically protected[36, 37]. Within the AB layer, there are only two ways to destroy these nodes. The first one is to generate a mass upon the massless Bogoliubov quasi-particles[38] which is forbidden by the TR symmetry in pairing sector. More precisely, the mass term for the Bogoliubov quasi-particles is additional pairing components with phase difference that can't be gauged away. The other way is to move the nodes with opposite vorticity to annihilate each other, which is prevented by the C_4^p symmetry that confines the nodes to the unfolded BZ diagonal.

Now we have two pairing components $\Delta_0(\mathbf{k})$ and $\Delta_{1s}(\mathbf{k})$ that can be varied by the NN interaction J_1 for a fixed NNN interaction $J_{2s} \equiv \frac{2J_2J'_2}{J_2+J'_2} \simeq 0.3$. The detailed self-consistency calculation explicitly shows phase transitions of pairing symmetry displayed in Fig.3. When $J_1 \ll J_{2s}$, the NNN interaction overwhelms the NN interaction, leading to the $s_{x^2-y^2}$ -wave pairing, whereas $J_1 \gg J_{2s}$ results in the $d_{x^2-y^2} \times s_{x^2+y^2}$ -wave pairing. In between, the SC with a mixed pairing $s + id \times s$ is energetically more favorable, which spontaneously breaks the TR symmetry. To compare with the pressure experiments[25], we notice that, upon increasing pressure, both t_2 and J_2 are expected to grow faster than t_1 and J_1 . Since the dopant concentration is fixed and the small hole pocket FS does not change qualitatively with t , we expect that decreasing the ratio of J_1/J_{2s} is adequate to capture the essential physics during the period of increasing pressure. On the other hand, from the perspective of low-energy dynamics, the phase transition from the $d \times s$ -wave nodal SC to the $s_{\pm} + id \times s$ nodeless SC belongs to the TR-breaking mass generation scenario of destroying the pairing gap nodes.

Being reminded of the CD layer, we can simply apply the S_4 symmetry to obtain its low-energy effective Hamiltonian:

$$H_{\text{eff}}^{\text{cd}} = \frac{1}{2} \sum_{\mathbf{k},\sigma} \xi_h(\mathbf{k}) \gamma_{\mathbf{k},\sigma}^\dagger \gamma_{\mathbf{k},\sigma} \quad (14)$$

$$+ \frac{\eta}{2} \sum_{\mathbf{k}} \left(\Delta_0(\mathbf{k}) + \frac{\epsilon_x(\mathbf{k})}{\sqrt{\epsilon_x^2 + \epsilon_z^2}} i \Delta_x(\mathbf{k}) \right) \gamma_{\mathbf{k},\uparrow}^\dagger \gamma_{-\mathbf{k},\downarrow}^\dagger + h.c.$$

where $\gamma_{\mathbf{k},\sigma}^\dagger = (\cos \frac{\theta_{\mathbf{k}}}{2}) c_{\mathbf{k},\sigma}^\dagger - \text{sgn}(\epsilon_x) (\sin \frac{\theta_{\mathbf{k}}}{2}) d_{\mathbf{k},\sigma}^\dagger$. η em-

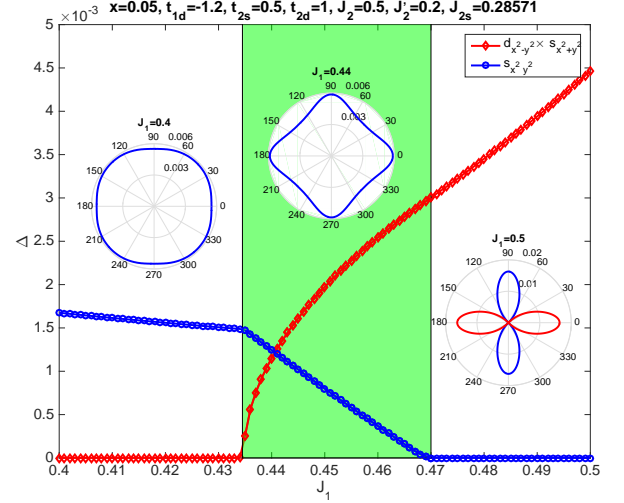


FIG. 3: Phase diagram of the superconducting phases for KFe₂As₂ under pressure (decreasing J_1 mimics the trend of increasing pressure). The $d_{x^2-y^2} \times s_{x^2+y^2}$ -wave SC comes to replace the $s_{x^2-y^2}$ -wave SC when J_1 overwhelms J_{2s} . The green color marks the intermediate phase region with $s_{x^2-y^2} + id_{x^2-y^2} \times s_{x^2+y^2}$ mixed pairing SC. Insets show the pairing gap symmetry on the FS, characteristic of the three pairing phases, respectively.

bodies the global phase difference between the pairing condensates of the two layers, and is restricted to be either ± 1 or $\pm i$ as the one-dimensional representations of the S_4 point group[29]. Nevertheless, the ambiguity of the phase difference can be eliminated by arbitrarily weak inter-layer interaction. Given an infinitesimal inter-layer NN or NNN AF super-exchange interaction, there appear inter-layer Cooper-pair scatterings in the momentum space with the strength $\propto -J_{1c}(\cos q_x + \cos q_y) - 2J_{2c}\cos q_x \cos q_y$. The important thing is that both hole pockets from the AB and CD layers are located near Γ point and are connected by long wave-length ($q \approx 0$) scatterings. As a result, the long wave-length inter-layer Cooper pair scatterings turn out to be attractive, locking the pairing phase between the two layers to be identical, i.e. $\eta = 1$. Then the nodes from the AB layer and those from the CD layer, which are related by S_4 and degenerate in the momentum space, turn out to carry opposite vorticity in the Nambu space. This naturally arouses worry as to whether they would "annihilate" each other. Nevertheless, this catastrophe could only happen when the inter-layer pairing is present. Otherwise, any inter-layer coupling outside the Nambu space, e.g. inter-layer tunneling is incapable of gapping out the degenerate nodes. The drastic distinction of these degenerate nodes from the usual accidental nodes, which always come easily to annihilate each other, is rooted in the multi-orbital character.

IV. OCTET NODAL SC FROM DISTORTING d -WAVE PAIRING

We are now in a good position to focus on the nodal phase at ambient pressure, which appears as a sphinx in a variety of experiments. Based on what we obtained, we have two S_4 -related C_4^p symmetric hole pockets which are absolutely degenerate. They can form d -wave pairing condensates with degenerate quartet nodes residing on the unfolded BZ diagonal (Fig.4a and 4b). Such degeneracy is highly unstable against any arbitrary perturbation, so we're obliged to return to real life modeling the more realistic materials by involving the weak C_4^p -breaking hopping t_{1s} and inter-layer tunneling t_c . As for the inter-layer tunneling, the s -wave NN tunneling would be the dominant term, from the estimate of orbitals overlap and symmetry analysis (see Fig.1b). Note that the on-site tunneling is suppressed because of the orbital orthogonality. Surprisingly, the S_4 symmetry survives this tunneling process. In our present theory, the inter-layer tunneling is required to be relatively weak compared to the C_4^p -breaking term, i.e. $|t_c| \ll |t_{1s}|$, otherwise it would strongly hybridize the two layers owing to their near degeneracy and lead to inter-layer Cooper pairs with the assistance of an infinitesimal inter-layer interaction. Such an assumption will be justified by our results that concur with the experiments. Therefore, the effective Hamiltonians for the AB and CD layers are modified by t_{1s} in their respective ways:

$$H_{\text{eff}}^{\text{ab}} = \frac{1}{2} \sum_{\mathbf{k},\sigma} \xi_h^+(\mathbf{k}) \beta_{\mathbf{k},\sigma}^\dagger \beta_{\mathbf{k},\sigma} + \frac{1}{2} \sum_{\mathbf{k}} \frac{\epsilon_{xd}(\mathbf{k}) + \epsilon_{xs}(\mathbf{k})}{\sqrt{(\epsilon_{xd} + \epsilon_{xs})^2 + \epsilon_z^2}} \Delta_x(\mathbf{k}) \beta_{\mathbf{k},\uparrow}^\dagger \beta_{-\mathbf{k},\downarrow}^\dagger + \text{h.c.} \quad (15)$$

$$H_{\text{eff}}^{\text{cd}} = \frac{1}{2} \sum_{\mathbf{k},\sigma} \xi_h^-(\mathbf{k}) \gamma_{\mathbf{k},\sigma}^\dagger \gamma_{\mathbf{k},\sigma} + \frac{1}{2} \sum_{\mathbf{k}} \frac{-\epsilon_{xd}(\mathbf{k}) + \epsilon_{xs}(\mathbf{k})}{\sqrt{(\epsilon_{xd} - \epsilon_{xs})^2 + \epsilon_z^2}} \Delta_x(\mathbf{k}) \gamma_{\mathbf{k},\uparrow}^\dagger \gamma_{-\mathbf{k},\downarrow}^\dagger + \text{h.c.} \quad (16)$$

where the global phase of Δ_{1s} is gauged to absorb the phase factor $-i$. Meanwhile, the normal state dispersion and the hybridization angle for AB/CD layer are given by

$$\xi_h^\pm = \epsilon_0 - \sqrt{(\epsilon_{xd} \pm \epsilon_{xs})^2 + \epsilon_z^2}, \quad (17)$$

and $\theta^\pm = \tan^{-1} \frac{|\epsilon_{xd} \pm \epsilon_{xs}|}{\epsilon_z} \in [0, \pi]$. As a result, the d -wave nodal lines that used to lie across the unfolded BZ diagonal are now twisted and dragged away from the Γ point by a "nematic force", resulting in a simultaneous movement of nodes along the elongating direction of the hole Fermi pockets (Fig.4a and 4b). Since the nodes with opposite vorticity need to travel a finite path along the FS before annihilation, they can survive a finite weak C_4^p -breaking term depending on the size of the FS.

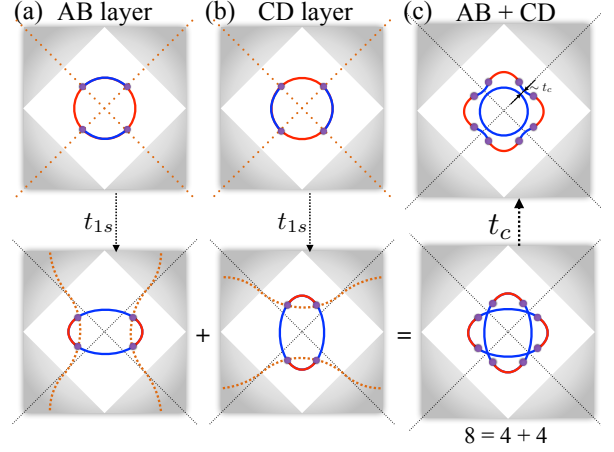


FIG. 4: Distorted d -wave nodes on the Fermi surfaces. The white diamond emphasizes the folded BZ; the orange dashed lines denote the nodal lines of the effective $d_{x^2-y^2}$ -wave pairing condensate on the FS distorted by $s_{x^2+y^2}$ -wave factor (the effect of weak s -wave is moderately exaggerated for illustration); The FS is separated by pairing nodal lines into the segments with positive (negative) pairing condensate marked by red (blue) color, respectively. (a) In the AB layer, the mixing weak s -wave NN hopping acts like a "nematic force" that elongates the FS and distorts the d -wave nodal lines, leading to shifted quartet nodes. (b) As the CD layer is related to AB layer by the S_4 symmetry, the distortion occurs in the perpendicular direction. (c) Near unfolded BZ diagonal the quasi-particles from the AB and CD layers are strongly hybridized with each other by any infinitesimal inter-layer tunneling. The intersecting elliptic hole pockets are therefore reconstructed into inner and outer pockets. The inner one has nodeless pairing gap whereas the outer one shows octet nodal gap structure. The origin of nodes can be attributed to a rather simple symbolic equation "8=4+4".

The hole pockets from the AB and CD layers are required by S_4 symmetry to intersect at the unfolded BZ diagonal (Fig.4c). Degeneracy at this point is unstable against any arbitrarily weak perturbation of inter-layer tunneling:

$$H_c = \frac{1}{2} \sum_{\mathbf{k},\sigma} \left[\epsilon_c(\mathbf{k}) \left(a_{\mathbf{k},\sigma}^\dagger d_{\mathbf{k},\sigma} + b_{\mathbf{k},\sigma}^\dagger c_{\mathbf{k},\sigma} \right) + \text{h.c.} \right] \rightarrow \frac{1}{2} \sum_{\mathbf{k},\sigma} \left[\tilde{\epsilon}_c(\mathbf{k}) \beta_{\mathbf{k},\sigma}^\dagger \gamma_{\mathbf{k},\sigma} + \text{h.c.} \right]. \quad (18)$$

So the degenerate Fermi-points at the unfolded BZ diagonal are split by $\tilde{\epsilon}_c(\mathbf{k})$ into two Fermi-points, whose corresponding quasi-particles are given by the bonding and anti-bonding states of the two layers. The split Fermi points smoothly join the Fermi sheets far away from the unfolded BZ diagonal, where $\tilde{\epsilon}_c(\mathbf{k})$ amounts only up to second order perturbation corrections (Fig.4c). Next let's consider how the pairing matrix changes with the inter-layer tunneling. Before inter-layer tunneling is turned on, the pairing condensates on the unfolded BZ diagonal

were identical for hole pockets from both layers, guaranteed by the S_4 symmetry. Hence the bonding of the two layers does not affect the pairing matrix along unfolded BZ diagonal, which maintains diagonal in the form of identity (see Appendix for detail). As a result, the two reconstructed bands yield the outer and inner hole pockets and are decoupled in pairing sector to the leading order. The outer pocket inherits the total octet nodes (Fig.4c), which still carry vorticity in the Nambu space and are protected by topology. On the inner pocket the pairing gap is nodeless. It should be made clear that our outer pocket corresponds to the "middle pocket" termed in experimental report [24], because the d_{xy} orbital has been neglected in our minimal model. In this picture, we can not only see how octet nodes come out naturally as observed in the laser ARPES[24], but can also understand why every two of the octet nodes in experiment are located so close to the unfolded BZ diagonal, because they are essentially born of the d -wave representation of C_4^p albeit distorted by the weak C_4^p -breaking term. Thus the so-called "octet-noded monster" is neither accidental nor some crazy Cooper pair of angular momentum as high as g -wave, but the combination of two distorted d -wave related by the S_4 symmetry. In short, the origin of nodes can be attributed to a symbolic equation " $8 = 4 + 4$ ". And the nodes share the same fate with the FS structure that protests against strong breaking of C_4^p symmetry.

V. CONCLUSION AND OUTLOOK

To conclude, by virtue of C_4^p and S_4 symmetries, we are able to sort out the tangling orbitals in a rational way. In KFe_2As_2 particularly, with a simple strong coupling minimal model, we reconcile the contradiction between the nodal gap structure and s -wave Cooper pairs in the presence of Γ hole Fermi pockets only. We also settle the disagreement between d -wave gap structure and the observation of octet nodes on one of the hole pockets. All in all, the key feature lies in the multi-orbital character. And the origin of nodes in this material can be attributed to a symbolic equation " $8 = 4 + 4$ " that tells a tale of two symmetries: " 4 " plays the role of the d -wave quartet nodes inherited from Fermi-surface structure stabilized by C_4^p , " $+$ " is guaranteed by the S_4 symmetry organizing two groups of orbitals, and the octet nodal gap is thus a natural result of the cooperation of these two symmetries. Besides simplicity, this organizing principle governed by C_4^p and S_4 symmetries is potentially universal in Fe-based superconductors. While the d -wave representation C_4^p of plaquette-centered rotation symmetry stabilizes the FS structure of iron-pnictides, the s -wave representation \tilde{C}_4^p captures the FS of iron-chalcogenides, where NN hopping is dominated by s -wave.

Inspired by the spirit of these considerations, we hope

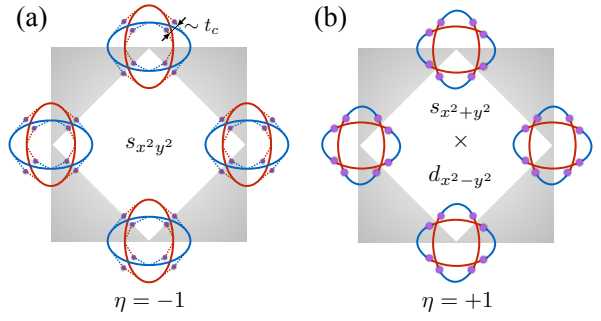


FIG. 5: Possible scenarios for gap structure of superconducting pairing of the monolayer FeSe on SrTiO_3 substrates. (a) When J_2 is dominant, both of the two layers are $s_{x^2-y^2}$ -wave pairing symmetry but differ by π phase. Any inter-layer tunneling t_c would reconstruct the FS leading to an outer and an inner electron pockets with nodes along folded BZ boundary. (b) When J_1 is dominant, the two layers have $s_{x^2+y^2} \times d_{x^2-y^2}$ -wave pairing symmetry without phase difference, where the nodes are distorted by \tilde{C}_4^p -breaking term.

to gain further insight into the pairing symmetry of iron-selenide (FeSe). We consider the monolayer FeSe with only electron Fermi pockets around X point [35], leaving behind the tiny hole pocket around Γ which is not robust and essential to reveal the SC mechanism. Parallel to the discussion for KFe_2As_2 above, there are two possible pairing symmetries for the monolayer FeSe in our consideration: one is the s_{\pm} -wave Cooper pair which is glued by the dominant NNN AF superexchange J_2 ; the other one is the effective $s_{x^2+y^2} \times d_{x^2-y^2}$ -wave Cooper pair on the electron pockets around the X point due to a relatively large NN AF superexchange. Note that the inter-orbital Cooper pair glued by J_1 has $d_{x^2-y^2}$ -wave symmetry whose nodal line avoids the FS to maximize energy gain, but the projection of this inter-orbital Cooper pair onto the FS yields additional $s_{x^2+y^2}$ form factor inherited from the orbital hybridization. The two possible pairing symmetries are competing, but the exact phase transition point needs more careful considerations. Since it is more intricate to pin down the one-dimensional representation of S_4 symmetry in FeSe, we therefore leave both possibilities $\eta = \pm 1$ under considerations. Among the four possible scenarios in total, two scenarios yield the gap structure that qualitatively agrees with the recent ARPES experimental results[35], which found a sphinx-like gap feature that is neither d -wave nor s -wave nor s_{\pm} -wave. As shown in Fig.5a and Fig.5b, the gap structure of the outer electron pocket in both scenarios yields the gap minimum near the folded BZ boundary and the gap maximum near the folded BZ diagonal. In fact, these two concrete scenarios not only agree with the experimental features but also surprisingly concur with the two crude speculations to explain the gap anisotropy[35]. Actually our theory has indicated that it is the value of J_1/J_2 that selects the realistic one from the two scenarios. More de-

tail considerations and calculations on FeSe are left for future study.

Acknowledgment.- GMZ acknowledges the support of National Key Research and Development Program of China (2016YFA0300300).

[1] J. P. Bednorz and K. A. Muller, *Z. Phys. B* **64**, 189 (1986).

[2] P. W. Anderson, *Science* **235**, 1196 (1987).

[3] P. W. Anderson, P. A. Lee, M. Randeria, T. M. Rice, N. Trivedi, and F. C. Zhang, *J. Phys. Condens. Matter* **16**, R755 (2004).

[4] P. A. Lee, N. Nagaosa, and X. G. Wen, *Rev. Mod. Phys.* **78**, 17 (2006).

[5] Z. X. Shen, D. S. Dessau, B. O. Wells, D. M. King, W. E. Spicer, A. J. Arko, D. Marshall, L. W. Lombardo, A. Kapitulnik, P. Dickinson, S. Doniach, J. DiCarlo, T. Loeser, and C. H. Park, *Phys. Rev. Lett.* **70**, 1553 (1993).

[6] D. A. Wollman, D. J. Van Harlingen, W. C. Lee, et al, *Phys Rev Lett.* **71**, 2134 (1993)

[7] C. C. Tsuei, J. R. Kirtley, C. C. Chi, L. S. Yuahnes, A. Gutpa, T. Shaw, J. Z. Sun, and M. B. Ketchen, *Phys. Rev. Lett.* **73**, 593 (1994).

[8] F. C. Zhang, and T. M. Rice, *Phys. Rev. B* **37**, 3759 (1988).

[9] G. Kotliar and J. Liu, *Phys. Rev. B* **38**, 5142 (1988).

[10] B. E. C. Koltenbah and R. Joynt, *Rep. Prog. Phys.* **60**, 23 (1997) and references therein.

[11] For recent reviews see J. P. Paglione and R. L. Greene, *Nat. Phys.* **6**, 645 (2010); I. I. Mazin, *Nature (London)* **464**, 183 (2010); D. N. Basov and A. V. Chubukov, *Nat. Phys.* **7**, 272 (2011); P. J. Hirschfeld, M. M. Korshunov, and I. I. Mazin, *Rev. Prog. Phys.* **74**, 124508 (2011); A. V. Chubukov, *Annu. Rev. Condens. Matter Phys.* **3**, 57 (2012); R. M. Fernandes, A. V. Chubukov, and J. Schmalian, *Nat. Phys.* **10**, 97 (2014).

[12] T. Terashima, M. Kimata, N. Kurita, H. Satsukawa, A. Harada, K. Hazama, M. Imai, A. Sato, K. Kihou, C.-H. Lee, H. Kito, H. Eisaki, A. Iyo, T. Saito, H. Fukazawa, Y. Kohori, H. Harima, and S. Uji, *J. Phys. Soc. Jpn.* **79**, 053702 (2010).

[13] T. Sato, K. Nakayama, Y. Sekiba, P. Richard, Y.-M. Xu, S. Souma, T. Takahashi, G. F. Chen, J. L. Luo, N. L. Wang, and H. Ding, *Phys. Rev. Lett.* **103**, 047002 (2009).

[14] S. Graser, T. A. Maier, P. J. Hirschfeld, and D. J. Scalapino, *New J. Phys.* **11**, 025016 (2009).

[15] K. J. Seo, B. A. Bernevig and J. Hu, *Phys. Rev. Lett.* **101**, 206404 (2008).

[16] R. Yu, J. Zhu, and Q. Si, *Phys. Rev. Lett.* **89**, 024509 (2014).

[17] J. K. Dong, S. Y. Zhou, T. Y. Guan, H. Zhang, Y. F. Dai, X. Qiu, X. F. Wang, Y. He, X. H. Chen, and S. Y. Li, *Phys. Rev. Lett.* **104**, 087005 (2010).

[18] K. Hashimoto, A. Serafin, S. Tonegawa, R. Katsumata, R. Okazaki, T. Saito, H. Fukazawa, Y. Kohori, K. Kihou, C. H. Lee, A. Iyo, H. Eisaki, H. Ikeda, Y. Matsuda, A. Carrington, and T. Shibauchi, *Phys. Rev. B* **82**, 014526 (2010).

[19] H. Fukazawa, Y. Yamada, K. Kondo, T. Saito, Y. Kohori, K. Kuga, Y. Matsumoto, S. Nakatsuji, H. Kito, P.M. Shirage, K. Kihou, N. Takeshita, C.-H. Lee, A. Iyo, and H. Eisaki, *J. Phys. Soc. Jpn.* **78**, 083712 (2009).

[20] S. W. Zhang, L. Ma, Y. D. Hou, J. Zhang, T.-L. Xia, G. F. Chen, J. P. Hu, G. M. Luke, and W. Yu, *Phys. Rev. B* **81**, 012503 (2010).

[21] Y. P. Wu, D. Zhao, A. F. Wang, N. Z. Wang, Z. J. Xiang, X. G. Luo, T. Wu, and X. H. Chen, *Phys. Rev. Lett.* **116**, 147001 (2016)

[22] R. Thomale, C. Platt, W. Hanke, J. Hu and B. A. Bernevig, *Phys. Rev. Lett.* **107**, 117001 (2011).

[23] J. P. Reid, M. A. Tanatar, A. Juneau-Fecteau, R. T. Gordon, S. Rende Cotret, N. Doiron-Leyraud, T. Saito, H. Fukazawa, Y. Kohori, K. Kihou, C. H. Lee, A. Iyo, H. Eisaki, R. Prozorov, and Louis Taillefer, *Phys. Rev. Lett.* **109**, 087001 (2012).

[24] K. Okazaki, Y. Ota, Y. Kotani, W. Malaeb, Y. Ishida, T. Shimojima, T. Kiss, S. Watanabe, C.-T. Chen, K. Kihou, C. H. Lee, A. Iyo, H. Eisaki, T. Saito, H. Fukazawa, Y. Kohori, K. Hashimoto, T. Shibauchi, Y. Matsuda, H. Ikeda, H. Miyahara, R. Arita, A. Chainani and S. Shin, *Science* **337** (6100), 1314-1317 (2012).

[25] F. F. Tafti, A. Juneau-Fecteau, M-E Delage, S. Rene de Cotret, J-Ph. Reid, A. F. Wang, X-G. Luo, X. H. Chen, N. Doiron-Leyraud and Louis Taillefer, *Nature Physics* **9**, 349-352 (2013).

[26] F. Hardy, A. E. Boehmer, D. Aoki, P. Burger, T. Wolf, P. Schweiss, R. Heid, P. Adelmann, Y. X. Yao, G. Kotliar, J. Schmalian, and C. Meingast, *Phys. Rev. Lett.* **111**, 027002 (2013).

[27] M. Nakajima, S. Ishida, T. Tanaka, K. Kihou, Y. Tomioka, T. Saito, C. -H. Lee, H. Fukazawa, Y. Kohori, T. Kakeshita, A. Iyo, T. Ito, H. Eisaki, and S. Uchida, *J. Phys. Soc. Jpn.* **83**, 104702 (2014).

[28] D. Podolsky, *Physics* **5**, 61 (2012).

[29] J. Hu and N. Hao, *Phys. Rev. X* **2**, 021009 (2012).

[30] D. Liu, W. Zhang, D. Mou, J. He, Y.-B. Ou, Q.-Y. Wang, Z. Li, L. Wang, L. Zhao, S. He, Y. Peng, X. Liu, C. Chen, L. Yu, G. Liu, X. Dong, J. Zhang, C. Chen, Z. Xu, J. Hu, X. Chen, X. Ma, Q. Xue, X. J. Zhou, *Nature Commun.* **3**, 931 (2012).

[31] S. Y. Tan, M. Xia, Y. Zhang, Z. R. Ye, F. Chen, X. Xie, R. Peng, D. F. Xu, Q. Fan, H. C. Xu, J. Juan, T. Zhang, X. C. Lai, T. Xiang, J. P. Hu, B. P. Xie, D. L. Feng, *Nature Mater.* **12**, 634 (2013).

[32] L. Fu and C. L. Kane, *Phys. Rev. Lett.* **100**, 096407 (2008).

[33] V. Grinenko, P. Materne, R. Sarkar, H. Luetkens, K. Kihou, C. R. Lee, S. Akhmadaliev, D. V. Efremov, S. L. Drechsler, and H. H. Klauss, *Phys. Rev. B* **95**, 214511 (2017).

[34] Y. Ran, F. Wang, H. Zhai, A. Vishwanath, and D. -H. Lee, *Phys. Rev. B* **79**, 014505 (2009).

[35] Y. Zhang, J. J. Lee, R. G. Moore, W. Li, M. Yi, M. Hashimoto, D. H. Lu, T. P. Devereaux, D. H. Lee and Z. X. Shen, *Phys. Rev. Lett.* **117**, 117001(2016).

[36] F. Wang and D. -H. Lee, *Phys. Rev. B* **86**, 094512 (2012).

[37] G. Y. Zhu, G. M. Zhang, *Europhys. Lett.* **117**, 67007 (2017).

[38] G. Y. Zhu, G. M. Zhang, *Europhys. Lett.* **118**, 37004 (2017).

APPENDIX A: GAUGE CHOICE FOR IRON-CHALCOGENIDES

The electronic structures of iron-pnictides and iron-chalcogenides could possibly be related by a gauge transformation followed by a particle-hole transformation. The candidate gauge choice for iron-chalcogenides is shown in Fig.6, which corresponds to the s -wave representation of plaquette-centered rotation symmetry i.e. $\tilde{C}_4^p = \tau_{31}$:

$$S_4 : \begin{pmatrix} A_{\mathbf{k},\sigma} \\ B_{\mathbf{k},\sigma} \\ C_{\mathbf{k},\sigma} \\ D_{\mathbf{k},\sigma} \end{pmatrix} \rightarrow \begin{pmatrix} C_{\mathbf{k}',\sigma} \\ D_{\mathbf{k}',\sigma} \\ -A_{\mathbf{k}',\sigma} \\ -B_{\mathbf{k}',\sigma} \end{pmatrix} = i\tau_{20} \begin{pmatrix} A_{\mathbf{k}',\sigma} \\ B_{\mathbf{k}',\sigma} \\ C_{\mathbf{k}',\sigma} \\ D_{\mathbf{k}',\sigma} \end{pmatrix},$$

$$\tilde{C}_4^p : \begin{pmatrix} A_{\mathbf{k},\sigma} \\ B_{\mathbf{k},\sigma} \\ C_{\mathbf{k},\sigma} \\ D_{\mathbf{k},\sigma} \end{pmatrix} \rightarrow \begin{pmatrix} B_{\mathbf{k}',\sigma} \\ A_{\mathbf{k}',\sigma} \\ -D_{\mathbf{k}',\sigma} \\ -C_{\mathbf{k}',\sigma} \end{pmatrix} = \tau_{31} \begin{pmatrix} A_{\mathbf{k}',\sigma} \\ B_{\mathbf{k}',\sigma} \\ C_{\mathbf{k}',\sigma} \\ D_{\mathbf{k}',\sigma} \end{pmatrix}.$$

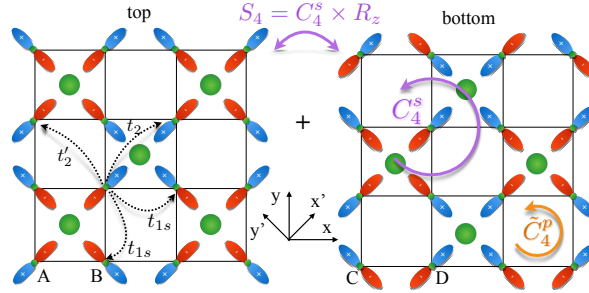


FIG. 6: Gauge choice for the iron-chalcogenides. An additional particle-hole transform is in need to get the correct FS structure for iron-chalcogenides.

APPENDIX B: QUASIPARTICLE SPECTRUM & GROUND STATE ENERGY DENSITY

The mean-field Hamiltonian for AB layer can be diagonalized as

$$E_{\pm} = \pm \sqrt{\Delta_0^2 + \Delta_x^2 + \epsilon_0^2 + \epsilon_x^2 + \epsilon_z^2 \pm 2\sqrt{(\epsilon_x^2 + \epsilon_z^2)\epsilon_0^2 + \Delta_x^2\epsilon_z^2}}, \quad (19)$$

and the mean-field ground state energy density is expressed as

$$\langle f \rangle = - \int_{BZ} \frac{dk_x dk_y}{8\pi^2} (E_+ + E_-) - \mu x + \frac{8}{J_1} (\kappa_1^2 + \Delta_{1s}^2) + \frac{4}{J_2} (\kappa_{2s} + \kappa_{2d})^2 + \frac{4}{J'_2} (\kappa_{2s} - \kappa_{2d})^2 + \frac{4(J_2 + J'_2)}{J_2 J'_2} \Delta_{2s}^2. \quad (20)$$

Minimization of ground state energy leads to the self-consistent equations and the phase diagram can be calculated.

APPENDIX C: PAIRING MATRIX IN HELICITY BASIS

The electron and hole band quasi-particles that carry \pm helicity respectively are related with the original spinon by the unitary transformation:

$$\begin{pmatrix} \alpha_{\mathbf{k},\sigma}^\dagger & \beta_{\mathbf{k},\sigma}^\dagger \end{pmatrix} = \begin{pmatrix} a_{\mathbf{k},\sigma}^\dagger & b_{\mathbf{k},\sigma}^\dagger \end{pmatrix} \begin{pmatrix} \cos \frac{\theta^+}{2} & -\sin \frac{\theta^+}{2} \text{sgn}(\epsilon_{xd} + \epsilon_{xs}) \\ \sin \frac{\theta^+}{2} \text{sgn}(\epsilon_{xd} + \epsilon_{xs}) & \cos \frac{\theta^+}{2} \end{pmatrix},$$

$$\begin{pmatrix} \zeta_{\mathbf{k},\sigma}^\dagger & \gamma_{\mathbf{k},\sigma}^\dagger \end{pmatrix} = \begin{pmatrix} c_{\mathbf{k},\sigma}^\dagger & d_{\mathbf{k},\sigma}^\dagger \end{pmatrix} \begin{pmatrix} \sin \frac{\theta^-}{2} \text{sgn}(\epsilon_{xd} - \epsilon_{xs}) & -\cos \frac{\theta^-}{2} \\ \cos \frac{\theta^-}{2} & -\sin \frac{\theta^-}{2} \text{sgn}(\epsilon_{xd} - \epsilon_{xs}) \end{pmatrix}, \quad (21)$$

where $\theta_{\mathbf{k}}^{\pm} = \tan^{-1} \frac{|\epsilon_{xd} \pm \epsilon_{xs}|}{\epsilon_z} \in [0, \pi]$ is the hybridization angle for AB (CD) layer. Pairing sector can be rotated to this helicity basis as follows,

$$\begin{aligned} H_{\Delta}^{\text{ab}} &= \frac{1}{2} \sum_{\mathbf{k}} \left(\begin{array}{cc} a_{\mathbf{k},\uparrow}^{\dagger} & b_{\mathbf{k},\uparrow}^{\dagger} \end{array} \right) (\Delta_0 + i\Delta_x I_x) \left(\begin{array}{c} a_{-\mathbf{k},\downarrow}^{\dagger} \\ b_{-\mathbf{k},\downarrow}^{\dagger} \end{array} \right) + h.c. \\ &= \frac{1}{2} \sum_{\mathbf{k}} \left(\begin{array}{cc} \alpha_{\mathbf{k},\uparrow}^{\dagger} & \beta_{\mathbf{k},\uparrow}^{\dagger} \end{array} \right) \left(\begin{array}{cc} \text{sgn}(\epsilon_x) \sin \theta_{\mathbf{k}}^{\pm} i\Delta_x + \Delta_0 & \cos \theta_{\mathbf{k}}^{\pm} i\Delta_x \\ \cos \theta_{\mathbf{k}}^{\pm} i\Delta_x & -\text{sgn}(\epsilon_x) \sin \theta_{\mathbf{k}}^{\pm} i\Delta_x + \Delta_0 \end{array} \right) \left(\begin{array}{c} \alpha_{-\mathbf{k},\downarrow}^{\dagger} \\ \beta_{-\mathbf{k},\downarrow}^{\dagger} \end{array} \right) + h.c., \end{aligned} \quad (22)$$

which give rise to both intra-band pairings and inter-band pairings. But for the electron band above the Fermi level, we are only interested in the intra-hole-band pairing for the low energy physics.

APPENDIX D: INTER-LAYER TUNNELING IN HELICITY BASIS

Considering the leading term for the inter-layer tunneling, which is the NN *s*-wave hopping in the spinon basis, we rotate the coupling Hamiltonian into the helicity basis to derive the effective tunneling between low energy hole bands of the two layers:

$$\begin{aligned} H_c &= \frac{1}{2} \sum_{\mathbf{k},\sigma} \left(\begin{array}{cc} a_{\mathbf{k},\sigma}^{\dagger} & b_{\mathbf{k},\sigma}^{\dagger} \end{array} \right) \left(\begin{array}{cc} 0 & \epsilon_c \\ \epsilon_c & 0 \end{array} \right) \left(\begin{array}{c} c_{\mathbf{k},\sigma} \\ d_{\mathbf{k},\sigma} \end{array} \right) + h.c. \\ &= \frac{1}{2} \sum_{\mathbf{k},\sigma} \left(\begin{array}{cc} \alpha_{\mathbf{k},\sigma}^{\dagger} & \beta_{\mathbf{k},\sigma}^{\dagger} \end{array} \right) \epsilon_c \left(\begin{array}{cc} \cos \frac{\theta^+ - \text{sgn}(\epsilon_{xd}^2 - \epsilon_{xs}^2)\theta^-}{2} & \text{sgn}(\epsilon_{xd} + \epsilon_{xs}) \sin \frac{\theta^+ - \text{sgn}(\epsilon_{xd}^2 - \epsilon_{xs}^2)\theta^-}{2} \\ -\text{sgn}(\epsilon_{xd} + \epsilon_{xs}) \sin \frac{\theta^+ - \text{sgn}(\epsilon_{xd}^2 - \epsilon_{xs}^2)\theta^-}{2} & \cos \frac{\theta^+ - \text{sgn}(\epsilon_{xd}^2 - \epsilon_{xs}^2)\theta^-}{2} \end{array} \right) \left(\begin{array}{c} \zeta_{\mathbf{k},\sigma} \\ \gamma_{\mathbf{k},\sigma} \end{array} \right) + h.c. \end{aligned} \quad (23)$$

where $\epsilon_c(\mathbf{k}) = 2\tilde{t}_c(\cos k_x + \cos k_y)$. The renormalization factor of the effective inter-hole-band coupling is found to be $\tilde{\epsilon}_c(\mathbf{k})/\epsilon_c(\mathbf{k}) = \cos \frac{\theta^+ - \text{sgn}(\epsilon_{xd}^2 - \epsilon_{xs}^2)\theta^-}{2}$, which approaches 1 within most of the BZ except dropping fast to 0 at the vicinity of Γ . For example, along the unfolded BZ diagonal, $\tilde{\epsilon}_c/\epsilon_c(k_x = k_y) \simeq \left(1 + \left(\frac{\tilde{t}_{1s}}{\tilde{t}_{2d} \sin k_x \tan k_x}\right)^2\right)^{-1/2}$.

APPENDIX E: EFFECTS OF INTER-LAYER TUNNELING

Let's focus on the nodal phase of KFe₂As₂. Given $|t_c| \ll |t_{1s}|$, the weak inter-layer tunneling contributes only second order perturbative correction to most of Fermi sheets except near the unfolded BZ diagonal, where the two layers are degenerate as guaranteed by the S_4 symmetry. Hence, we should only be concerned with the inter-layer tunneling effect on the unfolded BZ diagonal. Situations differ by the relative pairing phase factor between the two layers η . For simplicity we denote $\xi_h^{\pm}(k_x = \pm k_y) = \epsilon_0 - \sqrt{\epsilon_{xs}^2 + \epsilon_z^2} \mp \xi$, and $\Delta_{\text{eff}}(k_x = \pm k_y) = \frac{\epsilon_{xs}}{\sqrt{\epsilon_{xs}^2 + \epsilon_z^2}} \Delta_h \equiv \Delta$. Then the effective Hamiltonian along unfolded BZ diagonal involving both AB and CD layers becomes

$$H_{\text{eff}}^{\text{eff}}(k_x = \pm k_y) = \frac{1}{2} \sum_{k_x = \pm k_y} \left(\begin{array}{cccc} \beta_{\mathbf{k},\uparrow}^{\dagger} & \gamma_{\mathbf{k},\uparrow}^{\dagger} & \beta_{-\mathbf{k},\downarrow} & \gamma_{-\mathbf{k},\downarrow} \end{array} \right) \left(\begin{array}{cccc} \xi & \tilde{\epsilon}_c & \Delta & 0 \\ \tilde{\epsilon}_c & \xi & 0 & \eta\Delta \\ \Delta & 0 & -\xi & -\tilde{\epsilon}_c \\ 0 & \eta\Delta & -\tilde{\epsilon}_c & -\xi \end{array} \right) \left(\begin{array}{c} \beta_{\mathbf{k},\uparrow} \\ \gamma_{\mathbf{k},\uparrow} \\ \beta_{-\mathbf{k},\downarrow} \\ \gamma_{-\mathbf{k},\downarrow} \end{array} \right). \quad (24)$$

Taken a closer look, the normal sector can be diagonalized in terms of bonding and anti-bonding states as

$$H_t^{\text{eff}}(k_x = \pm k_y) = \frac{1}{2} \sum_{k_x = \pm k_y, \sigma} \left(\begin{array}{cc} \frac{\beta_{\mathbf{k},\sigma}^{\dagger} + \gamma_{\mathbf{k},\sigma}^{\dagger}}{\sqrt{2}} & \frac{\beta_{\mathbf{k},\sigma}^{\dagger} - \gamma_{\mathbf{k},\sigma}^{\dagger}}{\sqrt{2}} \end{array} \right) \left(\begin{array}{cc} \xi + \tilde{\epsilon}_c & 0 \\ 0 & \xi - \tilde{\epsilon}_c \end{array} \right) \left(\begin{array}{c} \frac{\beta_{\mathbf{k},\sigma} + \gamma_{\mathbf{k},\sigma}}{\sqrt{2}} \\ \frac{\beta_{\mathbf{k},\sigma} - \gamma_{\mathbf{k},\sigma}}{\sqrt{2}} \end{array} \right). \quad (25)$$

The degenerate Fermi points at unfolded BZ diagonal is therefore split apart by $\tilde{\epsilon}_c$, with the reconstructed Fermi points composed of bonding and anti-bonding quasi-particles $\frac{1}{\sqrt{2}}(\beta_{\mathbf{k},\sigma}^{\dagger} \pm \gamma_{\mathbf{k},\sigma}^{\dagger})$, respectively. When it comes to the pairing channel, the rotated pairing matrix depends on the relative pairing phase between two layers:

$$H_{\Delta}^{\text{eff}}(k_x = \pm k_y) = \frac{1}{2} \sum_{k_x = \pm k_y} \left(\begin{array}{cc} \frac{\beta_{\mathbf{k},\uparrow}^{\dagger} + \delta_{\mathbf{k},\uparrow}^{\dagger}}{\sqrt{2}} & \frac{\beta_{\mathbf{k},\uparrow}^{\dagger} - \delta_{\mathbf{k},\uparrow}^{\dagger}}{\sqrt{2}} \end{array} \right) \Delta \left(\begin{array}{cc} \frac{1+\eta}{2} & \frac{1-\eta}{2} \\ \frac{1-\eta}{2} & \frac{1+\eta}{2} \end{array} \right) \left(\begin{array}{c} \frac{\beta_{-\mathbf{k},\downarrow}^{\dagger} + \delta_{-\mathbf{k},\downarrow}^{\dagger}}{\sqrt{2}} \\ \frac{\beta_{-\mathbf{k},\downarrow}^{\dagger} - \delta_{-\mathbf{k},\downarrow}^{\dagger}}{\sqrt{2}} \end{array} \right) + h.c. \quad (26)$$

In the main body of our paper, we pin down $\eta = 1$ for the KFe₂As₂, as a result inter-band pairing is absent while intra-band pairing remains Δ , and $E_{\pm}(k_x = k_y) = \sqrt{(\xi \pm \tilde{\epsilon}_c)^2 + \Delta^2}$. The reconstructed Fermi-points at the unfolded BZ diagonal are then gapped by pairing condensate Δ . The Fermi points at the unfolded BZ diagonal join smoothly with the Fermi

sheets far away from the unfolded BZ diagonal, which stay intact from the weak inter-layer tunneling to the leading order. Likewise for the pairing gap structure.
